Assessing the CFD applicability of chemical kinetic mechanisms for pure ammonia combustion

Martinsen, Esben; Bilde, Kasper Gram; Yin, Chungen

Published in:
Fuel

DOI (link to publication from Publisher):
10.1016/j.fuel.2025.137360

Publication date:
2026

Document Version
Publisher's PDF, also known as Version of record

Fuel 407 (2026) 137360

Contents lists available at ScienceDirect

Fuel

journal homepage: www.elsevier.com/locate/jfue

Full length article

Assessing the CFD applicability of chemical kinetic mechanisms for pure ammonia combustion

Esben Martinsen[a, b,*], Kasper Gram Bilde[b], Chungen Yin[a]

[a] Aalborg University, Department of Energy, Pontoppidanstræde 111, Aalborg, DK-9220, Denmark
[b] Alfa Laval Aalborg, Gasværksvej 21, Aalborg, DK-9000, Denmark

HIGHLIGHTS

- 11 reaction mechanisms were investigated using numerical 1D flame simulations.
- Species time scale was found to be important for the solution time of 1D flames.
- The reaction mechanisms found suitable for CFD had different unique trade-offs.

ARTICLE INFO

Keywords:
Ammonia
Combustion
Reaction mechanism
CFD
Reduced kinetics

ABSTRACT

Ammonia is a promising carbon-free fuel, but realising its potential for green energy requires combustion models that are both accurate and computationally efficient. While many reaction mechanisms have been proposed, few are designed with computational fluid dynamics (CFD) applications in mind. This study evaluates 11 mechanisms based on their predictions of laminar flame speed, peak flame temperature, NO emissions, computational cost, and minimum species timescales. One-dimensional flame simulations across equivalence ratios from 0.5 to 1.5 identified three different mechanisms as the most promising, though each showed trade-offs in computational cost, NO prediction, or laminar flame speed accuracy. Random forest regression showed that the minimum species time scale is a key factor for solution time, on par with the number of reactions. Mechanisms with OH* sub-mechanisms produced very short time scales, potentially limiting their CFD applicability. Overall, the results highlight the need to balance computational cost and accuracy in mechanism selection, and call for further development of reduced mechanisms that address CFD-relevant metrics, such as the minimum species time scale.

1. Introduction

Ammonia is a promising future fuel due to its ability to serve as a hydrogen carrier and energy carrier [1,2]. However, direct application of ammonia, instead of cracking ammonia into nitrogen and hydrogen, is not straightforward due to its unique characteristics compared to traditional fuels [3]. Despite poor combustion characteristics, ammonia combustion is still a topic with much ongoing research, since efficient cracking of ammonia into hydrogen still requires high temperatures or catalysts containing rare metals like ruthenium [4,5]. Modelling of ammonia combustion is essential for investigating strategies to overcome its unique characteristics and thereby realise its potential as a future fuel. Modern computational fluid dynamics (CFD) tools can predict combustion with good accuracy [6–8], and serve as valuable design aids. However, due to the high computational cost in terms of time for combustion CFD simulations [9], it is vital to consider the trade-off between accuracy and computational cost. Robust and computationally efficient reaction mechanisms are therefore critical for CFD-based design, as reaction mechanisms form the foundation of combustion modelling. Speed-up factors of up to 150 or more have also been observed for tabulation and reduction methods [10], highlighting the high proportion of the computational cost associated with chemical kinetics and the drawbacks of using costly detailed reaction mechanisms. Given these challenges, it is essential to evaluate existing mechanisms to assess their suitability for CFD.

Numerous ammonia combustion mechanisms have been proposed in recent research. Glarborg et al. [11] proposed a detailed reaction mechanism (DRM) for nitrogen chemistry in combustion, also including

* Corresponding author at: Aalborg University, Department of Energy, Pontoppidanstræde 111, Aalborg, DK-9220, Denmark.
Email address: esma@energy.aau.dk (E. Martinsen).

https://doi.org/10.1016/j.fuel.2025.137360
Received 23 September 2025; Received in revised form 20 October 2025; Accepted 26 October 2025
Available online 6 November 2025

ammonia oxidation, with 231 reactions and 39 species. However, this mechanism was found to overpredict laminar flame speed [12]. Okafor et al. [13] investigated NH_3/CH_4/Air combustion and proposed a mechanism with 356 reactions and 59 species with improved flame speed predictions. Han et al. [14] proposed an improved mechanism of earlier work for NH_3/N_2O/Air flames consisting of 298 reactions and 36 species. This mechanism was developed to account for the effect of N_2O on laminar flame speed, while also improving the predictive ability of general NH_3 combustion.

In contrast to the majority of the research into ammonia combustion, some recent work has also focused on reduced kinetics. In work by da Rocha et al. [12], three different reduced mechanisms were proposed, based on mechanisms in literature, with the mechanisms ranging from 21–24 species and 51–72 reactions. The new mechanisms were observed to maintain similar behaviour to the original mechanisms. Work on global reaction mechanisms remains limited, but examples include the mechanisms proposed by Lindstedt and Selim [15] with 10 species and 7, 5 or 4 reactions. However, with the development of new reduced mechanisms, metrics describing the reduction in computational cost are often not reported, either for the mechanism itself or in comparison with other reduced or detailed mechanisms in the literature.

Nevertheless, it is essential to evaluate the potential reduction in computational cost to determine the extent to which global and reduced reaction mechanisms can serve as effective means to lower computational demands for combustion CFD, either as alternatives to or in conjunction with other methods, such as artificial neural networks [16] or tabulation [17,18].

This study aims to assess the current capabilities of selected available mechanisms in terms of accuracy and computational cost, identify the best current candidates for CFD, and outline areas where further development is needed for reduced kinetics.

A selection of reduced and global reaction mechanism candidates is presented and compared against experimental data, detailed reaction mechanisms and one another. The comparison will be carried out by examining the laminar flame speed, flame temperature, ammonia fuel slip, and NO emissions for one-dimensional flame simulations, as these selected parameters are central to capturing the interaction between the flame chemical kinetics and the fluid flow in CFD simulations, and the resulting emissions.

2. Current mechanisms

A selection of reaction mechanisms can be seen in Table 1. These mechanisms have been selected based on the criterion that they are suitable for ammonia combustion, but do not include species and reactions for the combustion of carbon fuels, as this would greatly increase the number of species and reactions in the mechanisms. This can, for example, be seen in a mechanism proposed by Li et al. [19], which contains 957 and 420 reactions for detailed and reduced mechanisms, respectively, targeting $NH_3/H_2/CH_4$ mixtures. Additionally, the selection has been focused on investigating global and reduced mechanisms, while also including detailed reaction mechanisms for reference.

2.1. Detailed mechanisms

The mechanism by Mei et al. [20] is proposed as an improvement on previous work, for NH_3/O_2 combustion, by gathering and using experimental data for $NH_3/NO/N_2$ mixtures at 1 atm and 298 K, ranging over equivalence ratios (ϕ) from 1.1 to 1.9. The mechanism includes 38 species, with 4 of them being carbon species, which are only included for third-body collisions.

This mechanism was updated with a focus on laminar flame speed and species, and it was able to predict NH_3/Air combustion well in the fuel-lean to stoichiometric mixture range. Zhang et al. [21] proposed a mechanism with focus on capturing ignition delay time and laminar flame speed for pure NH_3 and NH_3/H_2 mixtures, with H_2 volume fractions between 0–70 % and equivalence ratios between 0.25 and 1. The main focus of the work was, however, on NH_3/H_2 mixtures based on jet-stirred reactor experimental data. Otomo et al. [22] developed an improved mechanism based on Song et al. [23] validated for ignition delay time for pure NH_3 combustion as well as laminar flame speed for both pure NH_3 and NH_3/H_2 mixtures. The validation was conducted over a wide range of equivalence ratios and pressures up to 5 atm for the flame speed. The first mechanism proposed by Stagni et al. [24] was focused on capturing low temperature oxidation behaviour of diluted NH_3. Despite this focus, it also achieved good agreement for laminar flame speed for NH_3/air flames at 1 atm and 298 K. The mechanism was then updated [25] to better capture laminar flame speed, ignition delay time, and species mole fractions of NH_3/H_2 mixtures.

2.2. Reduced and global mechanisms

Gotama et al. [26] proposed a base mechanism, based on work by Han et al. [27], with focus on laminar flame speed of NH_3/H_2/air flames at elevated pressures and fuel-rich conditions up to 0.5MPa and an equivalence ratio of 1.8. The mechanism was then reduced by removing reactions containing carbon species and reactions negligible to laminar flame speed. Liu et al. [28] developed reduced and optimised mechanisms for both pure NH_3 and NH_3/H_2 mixtures. The mechanisms were intended for CFD of internal combustion but were also validated for laminar flame speed, ignition delay time, and species concentration in jet-stirred reactors. The reduction and optimisation were done using a genetic algorithm, with computational cost as part of the focus, to avoid a stiff mechanism. Both [29,30] proposed reduced mechanisms for NH_3/H_2 mixtures intended for numerical applications like CFD. The mechanism by Nozari and Karabeyoğlu [29] focused on laminar flame speed and NO_x at high-pressure conditions and fuel-lean conditions, while the mechanism by Duynslaegher et al. [30] was proposed for spark ignition simulation, with focus on species concentrations and NO_x pathways at low-pressure conditions.

Yang et al. [31] developed an optimised global reaction mechanism consisting of a set of reactions that can be used as a 4-step mechanism for NH_3/H_2 mixtures or a 1-step mechanism for pure NH_3. This was done with a focus on laminar flame speed and flame temperature, using data from 5 selected detailed reaction mechanisms for development of the global reaction mechanism. This study will focus on the 1-step for ammonia with reaction denoted “AS” by Yang et al. [31] as well as the 4-step with reactions denoted “HS/A1/A2/A3” by Yang et al. [31].

3. Numerical method

For evaluation and comparison of reaction mechanisms, flame simulations have been carried out in Cantera 3.1.0 using the Python interface. This has been done using a multi-component approach for transport equations, however, the Soret effect (thermal diffusion) is not accounted for. Adiabatic boundary conditions are assumed, and radiative heat transfer is neglected.

3.1. Governing equations

The simulations are carried out at constant pressure as steady axisymmetric flows according to the following equations. The continuity equation is given by

$$\frac{\partial u\rho}{\partial z} = 0, \tag{1}$$

where u is the axial velocity, z is the axial coordinate, and ρ, the density, which is calculated using the ideal gas law as the equation of state.

The governing equation for energy is defined as

$$\rho c_p u \frac{\partial T}{\partial z} = \frac{\partial}{\partial z}\left(\lambda \frac{\partial T}{\partial z}\right) - \sum_k j_k \frac{\partial h_k}{\partial z} - \sum_k h_k W_k \dot{\omega}_k, \tag{2}$$

where T is the temperature, c_p is the specific heat, λ is the thermal conductivity, j_k is the diffusive mass flux for species k, h is the enthalpy, W is the molar weight and $\dot{\omega}$ is the molar production rate.

Table 1
Overview of selected mechanisms from current literature. Detailed mechanisms are listed at the top, followed by reduced and global reaction mechanisms. Species counts are given as total species, with the number of carbon species denoted in parentheses. For mechanisms including both a base mechanism and a further reduced model, the version investigated in this study is underlined. The main mixture for each mechanism is specified, including, when relevant, the hydrogen mole fraction, $X_{H_2}^{fuel}$, or the ammonia energy fraction in the fuel mixture, E_{NH_3}. The main flame conditions covered in numerical or experimental analysis are also provided.

Mechanism (Year)	Mixture	Species	Reactions	Conditions
Mei et al. [20] (2021)	$NH_3/NO/N_2$	38 (4)	265	$0.6 \leq \phi \leq 1.9$, 1 atm
Zhang et al. [21] (2021)	$NH_3/H_2/O_2/N_2$ (0-70 % $X_{H_2}^{fuel}$)	38 (4)	263	$0.2 \leq \phi \leq 1$, 1 atm
Otomo et al. [22] (2018)	NH_3/H_2/air (0-100 % $X_{H_2}^{fuel}$)	32	213	$0.6 \leq \phi \leq 2$, 1–30 atm
Stagni et al. [24] (2020)	NH_3/O_2/He	31	203	$0.5 \leq \phi \leq 2$, 1–30 atm
Stagni et al. [25] (2023)	$NH_3/H_2/O_2$/He (0-100 % $X_{H_2}^{fuel}$)	31	203	$0.6 \leq \phi_{N_2} \leq 1$, 1 atm
Gotama et al. [26] (2022)	NH_3/H_2/air (40 % $X_{H_2}^{fuel}$)	32 <u>26</u>	165 <u>119</u>	$0.8 \leq \phi \leq 1.8$, 0.1–0.5 MPa
Liu et al. [28] (2023)	NH_3/H_2/air (0-100 % $X_{H_2}^{fuel}$)	29 (4)	63	$0.8 \leq \phi \leq 1.4$, 1–10 atm
Nozari and Karabeyoğlu [29] (2015)	NH_3/H_2/air (20-100 % E_{NH_3})	21	91 <u>77</u>	$1 \leq \phi \leq 1.8$, 10–17 bar
Duynslaegher et al. [30] (2012)	$NH_3/H_2/O_2$/Ar (≈ 17–38 % $X_{H_2}^{fuel}$)	19	80	$0.9 \leq \phi \leq 1.1$, 60–120 mbar
Yang et al. [31] 4-step (2024)	NH_3/H_2/air (0-100 % $X_{H_2}^{fuel}$)	7	4	$0.5 \leq \phi \leq 2.5$, 1–5 atm
Yang et al. [31] 1-step (2024)	NH_3/air	4	1	$0.5 \leq \phi \leq 2.5$, 1–5 atm

Using the multi-component approach but neglecting the Soret effect, the diffusive mass flux is given as

$$j_k = \frac{\rho W_k}{\overline{W}^2} \sum_i W_i D_{ki} \frac{\partial X_i}{\partial z}, \tag{3}$$

where X is the mole fraction, $\overline{W}$ is the mean molar mass and D_{ki} is the multi-component diffusion coefficient for species k quantifying how gradients in species i contribute to diffusion of species k.

The governing equation for species is given by

$$\rho u \frac{\partial Y_k}{\partial z} = -\frac{\partial j_k}{\partial z} + W_k \dot{\omega}_k, \tag{4}$$

where Y_k is the mass fraction of species k.

3.2. Boundary conditions

The described governing equations are then applied to simulate freely propagating flames.

For these simulations, the inlet temperature and mixture are fixed, while the inlet velocity is determined as part of the solution to achieve a "floating" flame. The pressure is also kept constant.

Flames are simulated at 1 atm and an inlet temperature of 300 K, unless other conditions are stated, while inlet mixtures range between an equivalence ratio of 0.5 and 1.5. Computations are carried out with steps of 0.05 in equivalence ratio, resulting in a total of 21 datasets for each reaction mechanism. For the outlet, the following conditions are specified for the temperature and species

$$\left.\frac{\partial T}{\partial z}\right|_{outlet} = 0, \qquad \left.\frac{\partial Y_k}{\partial z}\right|_{outlet} = 0. \tag{5}$$

3.3. Grid independence

The one-dimensional computational grid used has been automatically refined according to the refinement criteria in Table 2 to control the resolution of solutions. For the expressions in the table, z_j is the grid coordinate at node j, x denotes any of the solved values (e.g., species mole fraction, temperature), while x' is the spatial derivative of x. Finally, max and min in the subscript denote the maximum and minimum values in the entire computational domain.

To ensure sufficient grid resolution, three different refinement levels have been chosen as seen from the values in Table 2. Solutions using these refinement levels are then compared via laminar flame speed and flame temperature for selected mechanisms in Fig. 1.

From Fig. 1, it can be seen that the difference between the various solutions is negligible for the most part. However, some disagreement is observed in the flame temperature for the 4-step mechanism by Yang et al. [31]. In this case, the coarse grid deviates from the remaining solutions in slightly fuel-lean conditions as well as in fuel-rich conditions. Nevertheless, the difference between the medium and fine solutions is negligible. For this reason, the medium refinement level, as provided in Table 2, will be used in all other presented results.

Table 2
Values and expressions for grid refinement. The expression for R is only given for the forward direction (increasing index j), but a corresponding expression is also used for the reverse direction, which is simply the reciprocal expression of the forward direction. The medium values, in bold, have been shown to ensure sufficient grid resolution based on Fig. 1, and will be used in the remaining results.

	Ratio, R_{max}	Slope, S_{max}	Curve, C_{max}
Value (Coarse)	3.0	0.060	0.100
Value (Medium)	**2.0**	**0.030**	**0.050**
Value (Fine)	2.0	0.015	0.025
Expression	$R = \frac{z_{j+1} - z_j}{z_j - z_{j-1}}$	$S = \frac{\lvert x_{j+1} - x_j \rvert}{x_{max} - x_{min}}$	$C = \frac{\lvert x'_{j+1} - x'_j \rvert}{x'_{max} - x'_{min}}$

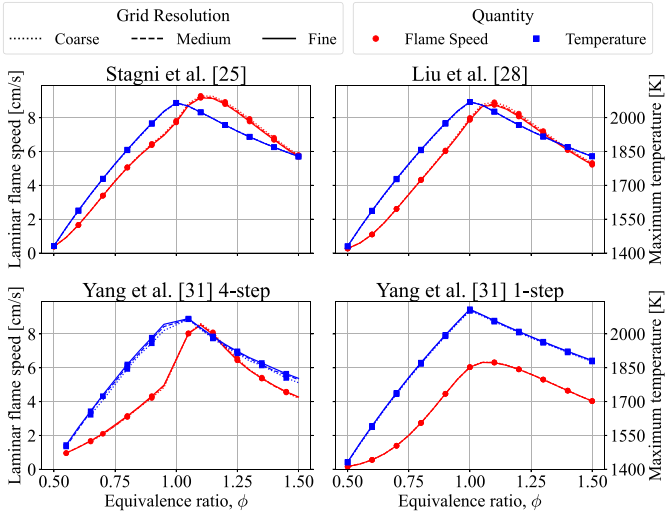

Fig. 1. Comparison of laminar flame speed and flame temperature for varying refinement of computational grid.

3.4. Species time scales

Combustion simulations via CFD involve a wide range of time scales as a consequence of modelling both three-dimensional fluid flow and chemistry. To make CFD simulations more feasible, it is desirable to limit the span of time scales, as short time scales and thereby a bigger span increase stiffness and consequently computational cost. For this reason, the species time scale will be evaluated for the flame simulations in order to assess their suitability for CFD. The used time scale for species is defined in Eq. (6) where C_k is the concentration of species k and $\dot{\omega}_k$ is the production rate. This metric has been selected, as it is simple to compute and allows identification of the species with the lowest time scales, which contribute most to increasing the span of time-scales required for modelling.

$$\tau_k = \frac{C_k}{\dot{\omega}_k} \tag{6}$$

From this definition, the minimum time scale, $\tau_k^{\min}$, will be found by checking time scales across all species throughout the entire solution domain and identifying the shortest time scale. Thus, each minimum time scale will have a corresponding species, temperature and location for which it occurs. In this manner, mechanisms and species with very short time scales can be highlighted, assisting in both evaluating current mechanisms and also potentially guiding future development of mechanisms suitable for CFD.

4. Results and discussion

4.1. Laminar flame speed

The flame speeds from the flame simulations can be seen for the different reaction mechanisms in Fig. 2. However, flame speeds from the mechanisms by Duynslaegher et al. [30] and Nozari and Karabeyoğlu [29] are not shown in the figure as these were found to far overestimate the laminar flame speed for NH_3/air mixtures. The mean error is more than 100 % with root mean square errors of more than 8 cm/s.

These deviations likely occur because the mechanisms were originally designed mainly with NH_3/H_2 mixtures in mind, as well as low and high pressures instead of atmospheric pressure, as seen from Table 1. For the mechanism proposed by Duynslaegher et al. [30], it is noted that the lowest investigated hydrogen fraction in the fuel is approximately 17 %, likely also contributing to the deviation.

Looking at the prediction of the remaining mechanisms in Fig. 2, good agreement is generally seen, however, there is a tendency for most mechanisms to overpredict the flame speed. This overprediction is partly due to the lack of radiation modelling in the free flame calculations, as resulting higher temperatures will cause a slightly elevated flame speed. It is also noted that there is generally less agreement between mechanisms for fuel-rich conditions, while the opposite is true for fuel-lean conditions. Both mechanisms by Yang et al. [31] are noted to be outliers from this, as they are close to or somewhat below experimental measurements. This is especially the case for the 1-step mechanism, which underpredicts the flame speed by approximately 1.9cm/s at an equivalence ratio of 1.1, when compared to experimental data by Mei et al. [33]. Additionally, the mechanism by Otomo et al. [22] is also noted to underpredict in the same way but to a lesser extent.

4.2. Maximum flame temperature

Comparing the maximum flame temperature predicted by the mechanisms in Fig. 3, it is seen that all mechanisms, except the mechanisms by Yang et al. [31], result in almost identical peak temperature predictions. However, even though the global reaction mechanisms by Yang et al. [31] deviate from remaining predictions, the maximum absolute percentage error (APE) from the mean is only 1.7 % and 2.9 % for the 4-step and 1-step mechanisms, respectively. This deviation may therefore

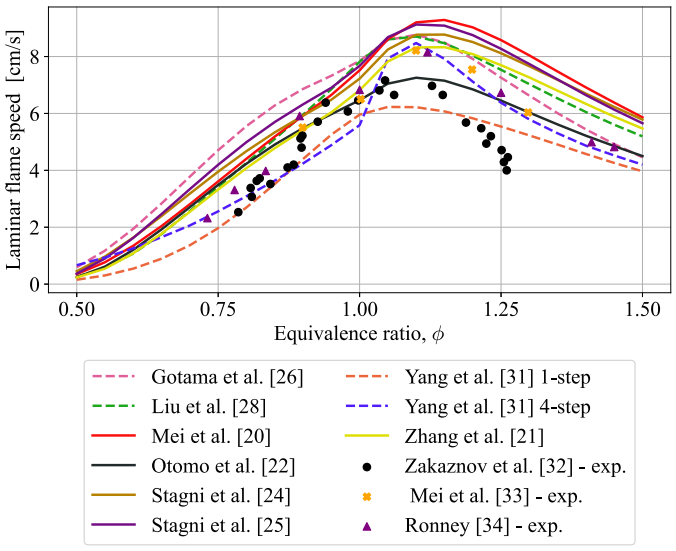

Fig. 2. Comparison of laminar flame speed for freely propagating flame at 1 atm and 298 K. Reduced mechanisms are plotted with dashed lines. Experimental data are shown for comparison [32–34].

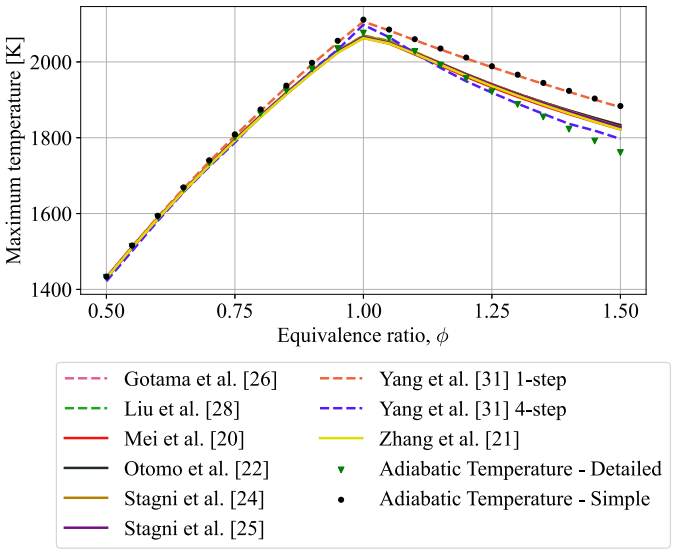

Fig. 3. Comparison of the maximum flame temperature for freely propagating flame at 1 atm and 300 K. Reduced mechanisms are plotted with dashed lines. Adiabatic flame temperatures were calculated using Gibbs free energy minimisation for two cases. A detailed equilibrium approach (using species from the mechanism by Stagni et al. [24]), where species such as NO and OH are among the products, and a simplified approach, where only N_2, H_2O, O_2, and NH_3 can appear as products, with the latter two only appearing for fuel-lean and fuel-rich mixtures, respectively.

be acceptable, depending on the application of the mechanism, especially for the 4-step mechanism, as the mean APE is only 0.73 %, which is caused solely by deviations at stoichiometric and fuel-rich conditions. It is also noted that the 1-step mechanism closely matches the simple adiabatic temperature, while the 4-step mechanism mostly follows the detailed adiabatic temperature, with some deviation at stoichiometric and fuel-rich conditions. The lower temperature of the 4-step mechanism is partly caused by a lower peak heat release rate. Comparing the 4-step mechanism to the mechanism by Stagni et al. [24] at an equivalence ratio of 1.4, the relative deviation is −1.79 % at the maximum temperature, as shown in Fig. 3, but the deviation at the final temperature at

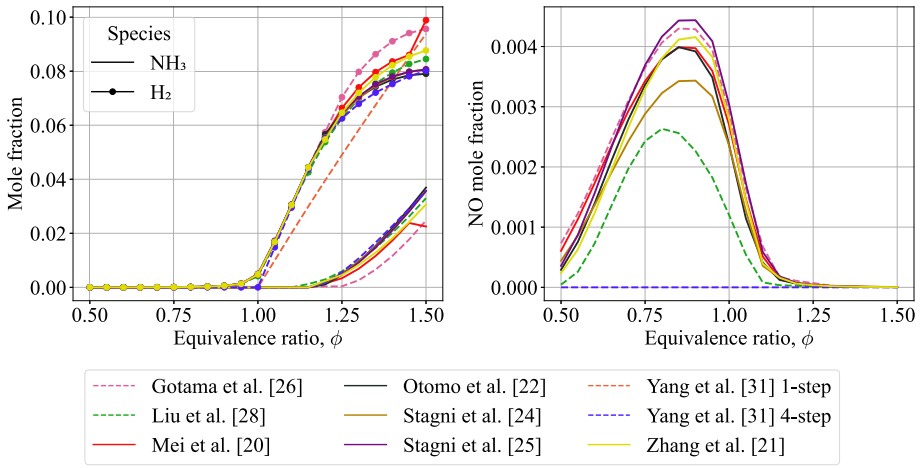

Fig. 4. Comparison for NH_3, H_2, and NO at the end of a freely propagating flame at 1 atm and 300 K. Reduced mechanisms are plotted with dashed lines.

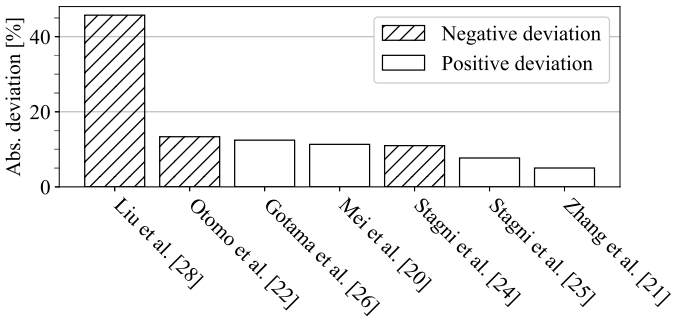

Fig. 5. Deviation of NO at end of flame simulation domain compared to experimental measurements of $NH_3/O_2/Ar$ flames by Osipova et al. [35] at $\phi = 1$. Simulations are carried out at atmospheric pressure and an inlet temperature of 383 K.

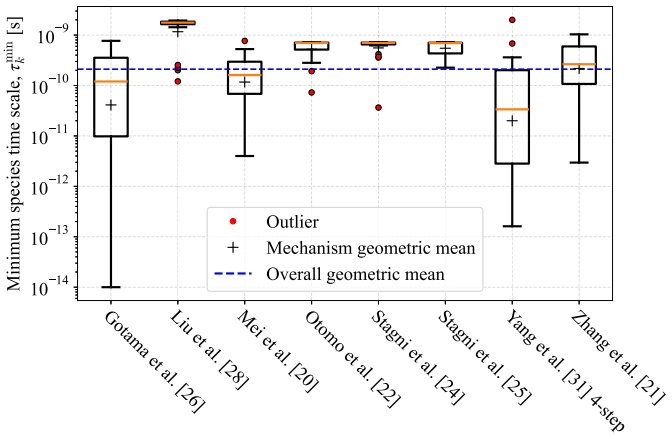

Fig. 6. Comparison of minimum species time scales via box plots for the different reaction mechanisms. The geometric mean of the minimum time scales across all mechanisms is illustrated by the dashed blue line, while crosses denote geometric means for the individual mechanisms.

the end of the flame was calculated to be only −0.85 %. However, when also factoring in the underprediction of laminar flame speed, the 1-step mechanism should likely be avoided if possible for most applications.

4.3. Species profiles

Comparing NH_3, H_2, and NO mole fractions at the end of the flame in Fig. 4, it can be seen that most of the mechanisms agree on NH_3 and H_2 slip up until an equivalence ratio of approximately 1.1. The 1-step mechanism by Yang et al. [31] is noted to be an outlier as it cannot account for NH_3 decomposition into H_2. It is also noted that even though NO is included in the 4-step mechanism by Yang et al. [31], it does not appear in the solution as it is fully consumed by the reaction NO+2H− > $0.5N_2 + H_2O$. Additionally, the mechanism by Mei et al. [20] is also seen to have an unusual jump in the predicted slip at equivalence ratios of 1.5.

For the prediction of NO, the majority of mechanisms also show fairly good agreement with each other, but with a wider spread of approximately up to 600 ppm difference. However, both the mechanism by Liu et al. [28] and the mechanism by Stagni et al. [24] have substantially lower predictions of NO. It is, however, noted that the improved mechanism by Stagni et al. [25] is more in line with the remaining mechanisms.

A similar trend in NO prediction can also be observed when comparing with experimental measurements of $NH_3/O_2/Ar$ flames by Osipova et al. [35], as evident from the deviation in Fig. 5. For this purpose, flame simulations have been conducted under conditions equivalent to the experimental setup. The NO mole fraction at the end of the computational domain has then been compared to the experimental measurements above the burner, where species mole fractions have stabilized. The deviations observed in Fig. 5 further confirm that the mechanism by Liu et al. [28] under-predicts NO emissions by more than 40 %. Mechanisms by Stagni et al.[25] and Zhang et al. [21] are found to result in the best prediction, while remaining mechanisms either overpredict or underpredict by approximately 10 %.

4.4. Applicability for CFD

In Fig. 6, the minimum species time scale, $\tau_k^{\min}$, as per Eq. (6) is shown to compare potential stiffness, which is important in the application case of CFD. It can be seen that the mechanisms by Gotama et al. [26], Mei et al. [20], and Yang et al. [31] are indicated to be most stiff, with more than 25 % of the simulation cases resulting in characteristic times below 1×10^{-10} s with worst cases ranging between 1×10^{-11} s and 1×10^{-14} s. It is noted that flame simulations using the 4-step mechanism by Yang et al. [31] required better initial guesses to ensure proper convergence, which indicates that $\tau_k^{\min}$ could be a useful metric to indicate robustness of mechanisms. The mechanism by Zhang et al. [21] is also noted to have only slightly better characteristic times than the mechanism by Mei et al. [20]. The mechanism by Liu et al. [28] is seen to have the longest characteristic times when disregarding outliers.

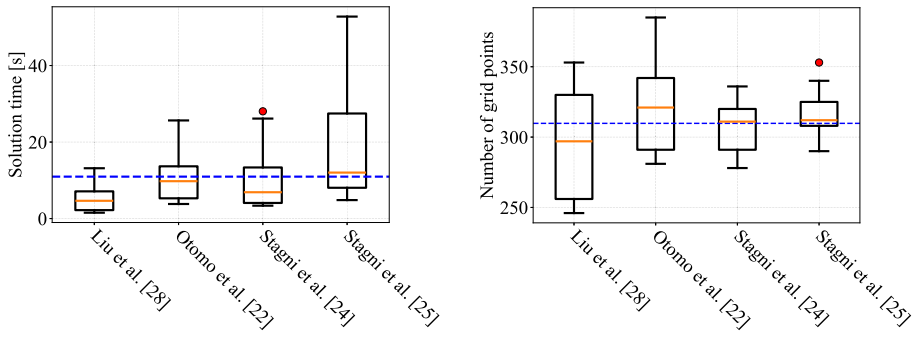

(a) Box plots of solution time for the different mechanisms. Simulations have been run in serial on an i7-13850HX CPU.

(b) Box plots of solution grid for the different mechanisms.

Fig. 7. Comparison of solution time and solution grids for the various mechanisms with box plots consisting of data points across equivalence ratios of 0.5 to 1.5. The arithmetic means across all data sets are shown in dashed blue lines.

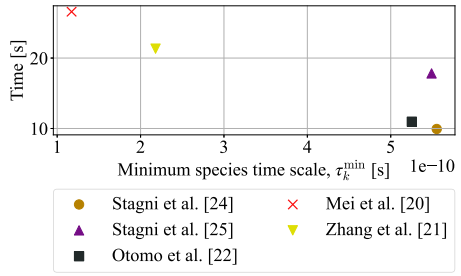

Fig. 8. Mean solution time depending on geometric mean of minimum characteristic species time, τ_k^{min}, for each detailed reaction mechanism.

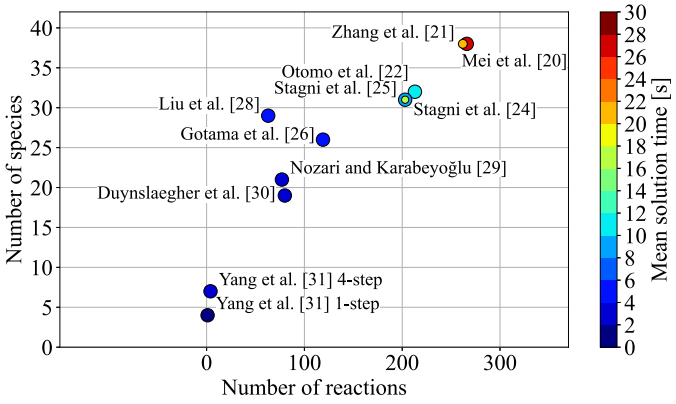

Fig. 9. Solution time of mechanisms shown alongside the number of reactions and species. The data dots for Stagni et al. [25] and Zhang et al. [21] have been made slightly smaller to ease the readability of overlapping points.

Based on Fig. 6, the mechanisms with time scales above the overall geometric mean (disregarding outliers) are deemed to be the better candidates for CFD implementation. It is also noted that the range of species time scales of the 4 mechanisms above the geometric mean is small compared to the remaining mechanisms, also suggesting more consistent behaviour, whereas the mechanism by Gotama et al. [26] has a large range, and may therefore still be an acceptable mechanism for some mixture conditions. In order to examine at the remaining suitable mechanisms, the computational time and number of required grid points are compared in Fig. 7. From the figure, it is seen that the mechanism by Liu et al. [28] is the least computationally expensive, while the mechanism by Stagni et al. [25] is the most expensive when comparing simulation times, and the mechanism by Otomo et al. [22] is the most expensive with regard to required spatial discretisation. However, the variation in the number of grid points is considerably lower than the variation in simulation time, as indicated by coefficients of variation (calculated as the ratio of the standard deviation to the mean across mechanisms) of 9 % and 87 % respectively.

It is noted from Fig. 7 that among the detailed reaction mechanisms, the mechanism with the lowest solution time, Stagni et al. [24] was also the mechanism with the generally higher τ_k^{min} value in Fig. 6. This tendency can also be seen in Fig. 8, where the mean solution time is plotted against the geometric mean of τ_k^{min} for each detailed reaction mechanism. Keeping in mind that the mechanisms also differ somewhat in the number of species and reactions, it is still noted that the tendency of increasing solution time with decreasing species time scale holds mostly, with only Stagni et al. [25] as an outlier.

4.5. Cause and importance of species time scale

The correlation between the number of species and reactions and solution time can be seen in Fig. 9. Here, it is seen that overall, there is a clear correlation with the increasing number of species and reactions, as expected. However, it is also seen that both the increase in computational time between mechanisms by Mei et al. [20] and Zhang et al. [21] is not explained, as well as the difference in computational time of the mechanisms by Stagni et al. [24,25] and Otomo et al. [22].

Referring back to Fig. 8, it is noted that these differences can be explained by the minimum species time scale, underlining the usefulness of the parameter for evaluating the mechanisms.

To quantify the predictiveness of the minimum time scale, a random forest regression was performed on 462 data points, consisting of two runs of 231 flame solutions, to create a model capable of estimating solution time. Two runs were used, as some variation in solution time was observed from run to run. The dataset was split randomly five times into a training and a test set, with the test sets containing 93 data points (~20 %). The random splits were done with different seeds to reduce the dependence of the results on any single split. The random forest models were trained on the remaining ~80 % of data points, using three features: the number of reactions, the number of species, and the minimum time scale. The training was based on 500 trees, each restricted to a maximum depth of 10. At each node split, all features were considered, and nodes were eligible for splitting if they contained at least two samples.

Across the five random splits, the trained models achieved mean R^2 scores of 0.966 with a standard deviation of 0.003 on the training sets and 0.882 with a standard deviation of 0.045 on the test sets.

In Fig. 10, the mean importance of the three features, across the five splits, is presented using two different approaches. The impurity-based

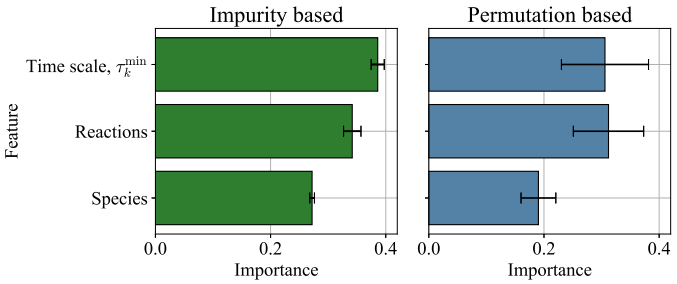

Fig. 10. Mean impurity and permutation-based feature importances for the random forest models. The standard deviations across the five data splits are given by the error bars.

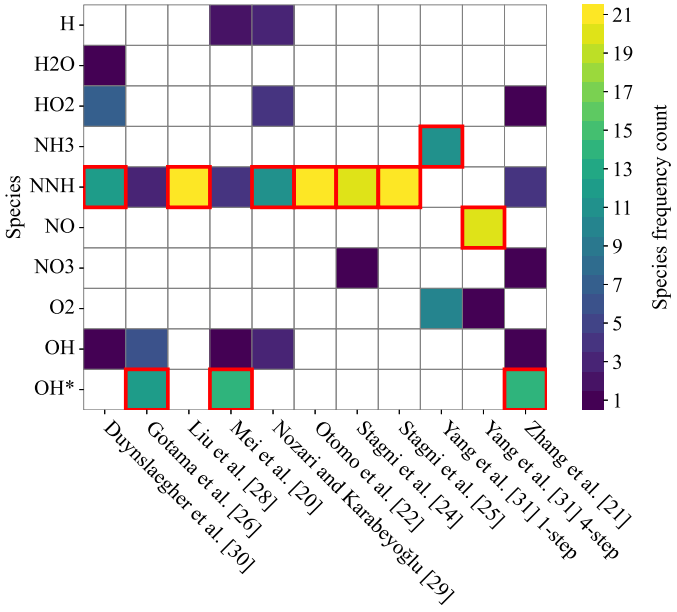

Fig. 11. The frequency count of species with minimum time scale across 21 flame solutions for each mechanism. The species observed most frequently are highlighted with a red outline for each mechanism.

approach quantifies feature importance by calculating the average reduction in prediction error contributed by each feature across all trees in the random forest model. The permutation-based approach computes importance by randomly shuffling one feature at a time in the test set and measuring the resulting decrease in model performance.

From Fig. 10, it can be seen, upon inspection, that there is a significant difference when comparing feature importance with the two methods. The number of reactions achieves the highest mean feature importance in the permutation-based approach, while it is outscored by the minimum time scale in the impurity-based approach. This suggests that even though the time scale is frequently used in splits in the random forest model, the number of reactions has an equivalent or higher impact on model predictions. However, the importances are seen to vary more for the permutation-based approach, as indicated by the error bars. It is also noted that the number of species ranks as the least important using both methods. However, as these feature importances are only based on the 11 mechanisms in Table 1, more comprehensive future investigations are still required to fully verify the importance of the minimum time scale.

In Fig. 11, the frequency at which species appear with the lowest time scale can be seen for the different mechanisms.

It is noted that NNH is seen to be most frequent across 6 mechanisms, with OH* observed most across 3 other mechanisms. NH_3 and NO are

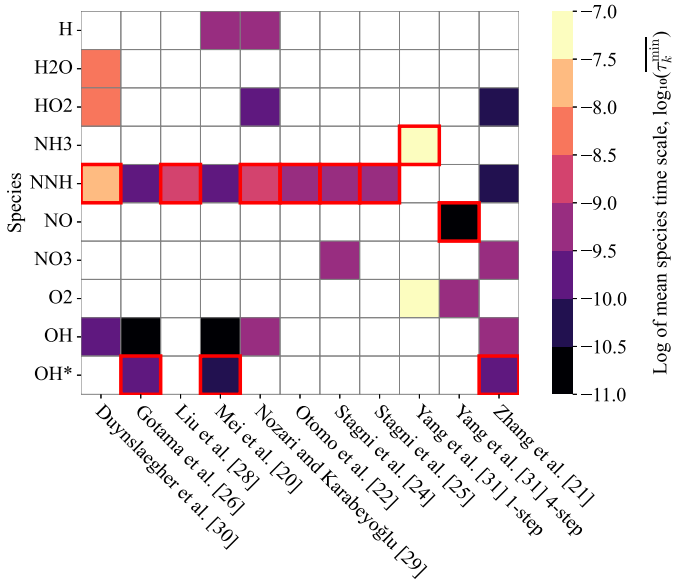

Fig. 12. Comparison of average minimum species time scale across mechanisms. The colourbar has been set with limits of −7 to −11 for best visualisation, but shorter and longer time scales do occur in some entries. The species observed most frequently are highlighted with a red outline for each mechanism.

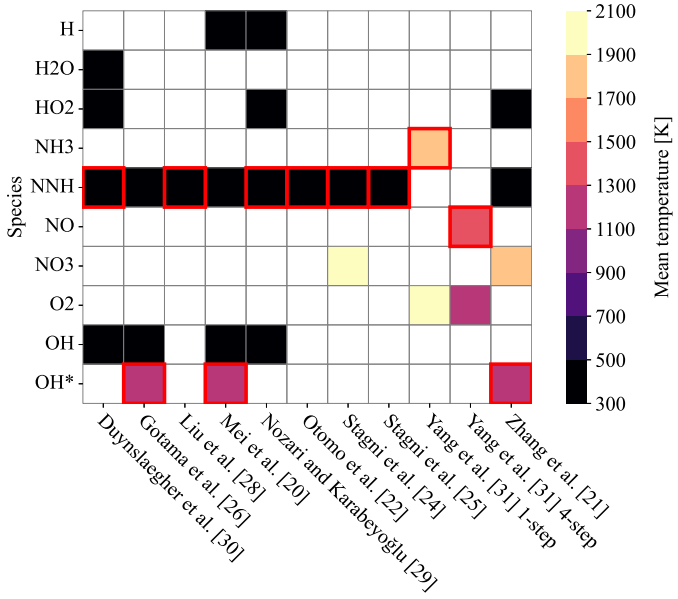

Fig. 13. Comparison of mean temperature at which species with minimum time scale occur. The species observed most frequently are highlighted with a red outline for each mechanism.

only observed in the special cases of the 1-step and 4-step mechanisms by Yang et al. [31] respectively.

In Fig. 12, the logarithm ($\log_{10}$) of the average time scale is shown to compare the time scales between species and mechanisms.

From Fig. 12, OH and NO are seen to be the species with the lowest time scales, ranging from 5.1×10^{-10} s to 8.5×10^{-13} s. OH* is however observed more frequently than OH but with a longer time scale. Finally, NNH is also seen to have fairly short time scales, but with a range of 6.6×10^{-11} s to 1.6×10^{-8} s across mechanisms.

Both mechanisms by Mei et al. [20] and Zhang et al. [21] include a sub-mechanism for OH* by Kathrotia et al. [36], while the mechanism

by Gotama et al. [26] uses a modified sub-mechanism based on work by Varga et al. [37]. Therefore, it may be straightforward to improve the stiffness of these mechanisms for use with CFD by leaving out the sub-mechanism, provided that the resulting reduction in accuracy is acceptable.

Fig. 13 shows the mean temperature at which the species appear in the solutions.

Low temperatures for both OH and NNH suggest a numerical issue, as they appear outside the highly reactive zones with negligible concentrations but relatively large production rates. However, this would still be desirable to avoid, to ease numerical computations. It is also noted that OH only appears as a short time scale species in 4 mechanisms, showing that these numerical issues can be avoided in some cases.

It is also seen that OH*, O_2, NO, NO_3 and NH_3 all occur in higher temperature zones. Among these OH* and NO may be most problematic due to their frequency and time scale as seen from Figs. 11 and 12. It is noted that the low time scale observed for NO in a high temperature area may simply be caused by tuning of activation energy and pre-exponential factor, carried out by Yang et al. [31], to improve laminar flame speed prediction accuracy.

5. Conclusion

Freely propagating flame simulations were carried out to evaluate the CFD suitability of 11 ammonia combustion reaction mechanisms. The mechanisms proposed by Liu et al. [28], Stagni et al. [25], and Otomo et al. [22] demonstrated the most promising performance across key metrics, including laminar flame speed, maximum flame temperature and minimum species time scale.

Each mechanism, however, had distinct trade-offs:

- The mechanism by Liu et al. [28] offered fast solution times and favourable species time scales, but significantly underpredicted NO emissions.
- The mechanism by Otomo et al. [22] resulted in better NO emission prediction but underpredicted flame speeds at stoichiometric conditions.
- The mechanism by Stagni et al. [25] had better NO emission prediction and predicted higher flame speeds, but at a greater computational cost and less favourable species time scales.

Random forest regression identified the minimum species time scale as an important feature for estimating solution time, being approximately equal in importance to the number of reactions, but surpassing the importance of the number of species. However, all three features contributed significantly to the solution time prediction.

The source of the low species time scale and thereby potential stiffness was found to differ among mechanisms. At low temperatures below 500 K OH and NNH were frequently observed as the lowest time scale species, likely due to numerical effects arising from negligible concentrations combined with relatively large production rates, with observed time scales ranging from 8.5×10^{-13} s to 1.6×10^{-8} s. In three mechanisms, OH* sub-mechanisms introduced a significant decrease in minimum time scale, suggesting that these may be undesirable to include in CFD simulations. The 4-step mechanism by Yang et al. [31] showed short time scales of 1.7×10^{-11}s associated with NO likely due to tuning of reaction rates to improve flame speed prediction accuracy.

These findings highlight the need to balance chemical accuracy with computational efficiency when selecting mechanisms for CFD. They also emphasise the need for further development of reduced mechanisms with explicit consideration of species time scales to ensure suitability for CFD applications. Future studies could build on these insights by establishing mechanism reduction frameworks that explicitly account for species time scales when selecting species and reactions for removal, and when determining the degree to which reactions should be tuned, for instance by adjusting the pre-exponential factor. Such an approach could lead to reduced mechanisms more effectively tailored for CFD applications.

CRediT authorship contribution statement

Esben Martinsen: Writing – review & editing, Writing – original draft, Visualization, Validation, Methodology, Investigation, Formal analysis, Conceptualization. **Kasper Gram Bilde:** Writing – review & editing, Supervision, Conceptualization. **Chungen Yin:** Writing – review & editing, Supervision, Conceptualization.

Declaration of generative AI and AI-assisted technologies in the writing process

During the preparation of this work, the authors used ChatGPT in order to improve selected sentence formulations. All content generated with the tool was carefully reviewed and edited by the authors, who take full responsibility for the final published article.

Declaration of competing interest

The authors declare that they have no known competing financial interests or personal relationships that could have appeared to influence the work reported in this paper.

Acknowledgements

This work was supported by the Innovation Fund Denmark [grant number 4365-00037B]. The funding source had no involvement in relation to the study design, collection, analysis and interpretation of data, writing of the report and decision to submit the article for publication.

Data availability

Data will be made available on request.

References

[1] Cardoso JS, Silva V, Rocha RC, Hall MJ, Costa M, Eusébio D. Ammonia as an energy vector: current and future prospects for low-carbon fuel applications in internal combustion engines. J Clean Prod 2021;296:126562. https://doi.org/10.1016/j.jclepro.2021.126562

[2] Kobayashi H, Hayakawa A, Somarathne KKA, Okafor EC. Science and technology of ammonia combustion. Proc Combust Inst 2019;37:109–33. https://doi.org/10.1016/j.proci.2018.09.029

[3] Elbaz AM, Wang S, Guiberti TF, Roberts WL. Review on the recent advances on ammonia combustion from the fundamentals to the applications. Fuel Commun 2022;10:100053. https://doi.org/10.1016/j.jfueco.2022.100053

[4] Asif M, Bibi SS, Ahmed S, Irshad M, Hussain MS, Zeb H, Khan MK, Kim J. Recent advances in green hydrogen production, storage and commercial-scale use via catalytic ammonia cracking. Chem Eng J 2023;473:145381. https://doi.org/10.1016/j.cej.2023.145381

[5] Lucentini I, Garcia X, Vendrell X, Llorca J. Review of the decomposition of ammonia to generate hydrogen. Ind Eng Chem Res 2021;60:18560–611. https://doi.org/10.1021/acs.iecr.1c00843

[6] Nakamura H, Zhang J, Hirose K, Shimoyama K, Ito T, Kanaumi T. Generating simplified ammonia reaction model using genetic algorithm and its integration into numerical combustion simulation of 1 mw test facility. Appl Energy Combust Sci 2023;15:100187. https://doi.org/10.1016/j.jaecs.2023.100187

[7] Füzesi D, Józsa V. The importance of unsteady phenomena of ammonia/methane combustion in an experimental swirl burner: comparison of steady-state and transient simulation results. Combust And Flame 2024;260:113207. https://doi.org/10.1016/j.combustflame.2023.113207

[8] Nassini PC, Pampaloni D, Meloni R, Andreini A. Lean blow-out prediction in an industrial gas turbine combustor through a les-based cfd analysis. Combust And Flame 2021;229:111391. https://doi.org/10.1016/j.combustflame.2021.02.037

[9] Raman V, Hassanaly M. Emerging trends in numerical simulations of combustion systems. Proc Combust Inst 2019;37:2073–89. https://doi.org/10.1016/j.proci.2018.07.121

[10] Contino F, Jeanmart H, Lucchini T, D'Errico G. Coupling of in situ adaptive tabulation and dynamic adaptive chemistry: an effective method for solving combustion in engine simulations. Proc Combust Inst 2011;33:3057–64. https://doi.org/10.1016/j.proci.2010.08.002

[11] Glarborg P, Miller JA, Ruscic B, Klippenstein SJ. Modeling nitrogen chemistry in combustion. Prog Energy Combust Sci 2018;67:31–68. https://doi.org/10.1016/j.pecs.2018.01.002

[12] da Rocha RC, Costa M, Bai X-S. Chemical kinetic modelling of ammonia/hydrogen/air ignition, premixed flame propagation and no emission. Fuel 2019;246:24–33. https://doi.org/10.1016/j.fuel.2019.02.102

[13] Okafor EC, Naito Y, Colson S, Ichikawa A, Kudo T, Hayakawa A, Kobayashi H. Experimental and numerical study of the laminar burning velocity of ch4–nh3–air premixed flames. Combust And Flame 2018;187:185–98. https://doi.org/10.1016/j.combustflame.2017.09.002
[14] Han X, Lavadera ML, Konnov AA. An experimental and kinetic modeling study on the laminar burning velocity of nh3 + n2o + air flames. Combust And Flame 2021;228:13–28. https://doi.org/10.1016/j.combustflame.2021.01.027
[15] Lindstedt RP, Selim MA. Reduced reaction mechanisms for ammonia oxidation in premixed laminar flames. Combust Sci Technol 1994;99:277–98. https://doi.org/10.1080/00102209408935437
[16] Zhang S, Zhang C, Wang B. Crk-pinn: a physics-informed neural network for solving combustion reaction kinetics ordinary differential equations. Combust And Flame 2024;269:113647. https://doi.org/10.1016/j.combustflame.2024.113647
[17] Pope S. Computationally efficient implementation of combustion chemistry using in situ adaptive tabulation. Combust Theory Model 1997;1:41–63. https://doi.org/10.1080/713665229
[18] Muto M. Tabulated chemistry models for numerical simulation of combustion flow field. Fluids 2025;10. https://doi.org/10.3390/fluids10040083
[19] Li R, Konnov AA, He G, Qin F, Zhang D. Chemical mechanism development and reduction for combustion of nh3/h2/ch4 mixtures. Fuel 2019;257:116059. https://doi.org/10.1016/j.fuel.2019.116059
[20] Mei B, Ma S, Zhang X, Li Y. Characterizing ammonia and nitric oxide interaction with outwardly propagating spherical flame method. Proc Combust Inst 2021;38:2477–85. https://doi.org/10.1016/j.proci.2020.07.133
[21] Zhang X, Moosakutty SP, Rajan RP, Younes M, Sarathy SM. Combustion chemistry of ammonia/hydrogen mixtures: jet-stirred reactor measurements and comprehensive kinetic modeling. Combust And Flame 2021;234:111653. https://doi.org/10.1016/j.combustflame.2021.111653
[22] Otomo J, Koshi M, Mitsumori T, Iwasaki H, Yamada K. Chemical kinetic modeling of ammonia oxidation with improved reaction mechanism for ammonia/air and ammonia/hydrogen/air combustion. Int J Hydrogen Energy 2018;43:3004–14. https://doi.org/10.1016/j.ijhydene.2017.12.066
[23] Song Y, Hashemi H, Christensen JM, Zou C, Marshall P, Glarborg P. Ammonia oxidation at high pressure and intermediate temperatures. Fuel 2016;181:358–65. https://doi.org/10.1016/j.fuel.2016.04.100
[24] Stagni A, Cavallotti C, Arunthanayothin S, Song Y, Herbinet O, Battin-Leclerc F, Faravelli T. An experimental, theoretical and kinetic-modeling study of the gas-phase oxidation of ammonia. React Chem Eng 2020;5:696–711. https://doi.org/10.1039/C9RE00429G
[25] Stagni A, Arunthanayothin S, Dehue M, Herbinet O, Battin-Leclerc F, Bréquigny P, Mounaïm-Rousselle C, Faravelli T. Low- and intermediate-temperature ammonia/hydrogen oxidation in a flow reactor: experiments and a wide-range kinetic modeling. Chem Eng J 2023;471:144577. https://doi.org/10.1016/j.cej.2023.144577
[26] Gotama GJ, Hayakawa A, Okafor EC, Kanoshima R, Hayashi M, Kudo T, Kobayashi H. Measurement of the laminar burning velocity and kinetics study of the importance of the hydrogen recovery mechanism of ammonia/hydrogen/air premixed flames. Combust And Flame 2022;236:111753. https://doi.org/10.1016/j.combustflame.2021.111753
[27] Han X, Wang Z, He Y, Zhu Y, Cen K. Experimental and kinetic modeling study of laminar burning velocities of nh3/syngas/air premixed flames. Combust And Flame 2020;213:1–13. https://doi.org/10.1016/j.combustflame.2019.11.032
[28] Liu X, Wang Y, Bai Y, Yang W. Development of reduced and optimized mechanism for ammonia/ hydrogen mixture based on genetic algorithm. Energy 2023;270:126927. https://doi.org/10.1016/j.energy.2023.126927
[29] Nozari H, Karabeyoğlu A. Numerical study of combustion characteristics of ammonia as a renewable fuel and establishment of reduced reaction mechanisms. Fuel 2015;159:223–33. https://doi.org/10.1016/j.fuel.2015.06.075
[30] Duynslaegher C, Contino F, Vandooren J, Jeanmart H. Modeling of ammonia combustion at low pressure. Combust And Flame 2012;159:2799–805. https://doi.org/10.1016/j.combustflame.2012.06.003
[31] Yang HM, Yeo JH, Kim NI. Optimized global reaction mechanism for h2 + nh3 + n2 mixtures. Int J Hydrogen Energy 2024;73:749–60. https://doi.org/10.1016/j.ijhydene.2024.06.102
[32] Zakaznov V, Kursheva L, Fedina Z. Determination of normal flame velocity and critical diameter of flame extinction in ammonia-air mixture. Combust Explos Shock Waves 1978;14:710–3. https://doi.org/10.1007/BF00786097
[33] Mei B, Zhang X, Ma S, Cui M, Guo H, Cao Z, Li Y. Experimental and kinetic modeling investigation on the laminar flame propagation of ammonia under oxygen enrichment and elevated pressure conditions. Combust And Flame 2019;210:236–46. https://doi.org/10.1016/j.combustflame.2019.08.033
[34] Ronney PD. Effect of chemistry and transport properties on near-limit flames at microgravity. Combust Sci Technol 1988;59:123–41. https://doi.org/10.1080/00102208808947092
[35] Osipova KN, Korobeinichev OP, Shmakov AG. Chemical structure and laminar burning velocity of atmospheric pressure premixed ammonia/hydrogen flames. Int J Hydrogen Energy 2021;46:39942–54. https://doi.org/10.1016/j.ijhydene.2021.09.188
[36] Kathrotia T, Fikri M, Bozkurt M, Hartmann M, Riedel U, Schulz C. Study of the h + o + m reaction forming oh*: kinetics of oh* chemiluminescence in hydrogen combustion systems. Combust And Flame 2010;157:1261–73. https://doi.org/10.1016/j.combustflame.2010.04.003
[37] Varga T, Olm C, Nagy T, Zsély IG, Valkó É, Pálvölgyi R, Curran HJ, Turányi T. Development of a joint hydrogen and syngas combustion mechanism based on an optimization approach. Int J Chem Kinet 2016;48:407–22. https://doi.org/10.1002/kin.21006